Chapter 3

Analysis Techniques and Film Deposition

In this chapter, the analysis methods are described. Section 3.1 is a summary of the relevant analysis techniques used in the later chapters of this dissertation. Section 3.2 is the description of the ion beam deposition system and its advantage.

3.1 Analysis Techniques

In this section, the analysis techniques are divided into three parts: (1). magnetic measurements, (2). transport measurements, and (3). material and structural characterizations.

TSING HUA UNIVERSITY

3.1.a Magnetic Measurements

In our studies, magnetic properties were measured by magneto-optical Kerr effect (MOKE) and vibrating sample magnetometer (VSM). The operation principles of MOKE and VSM are described as the following:

Magneto-Optical Kerr Effect (MOKE)

Fig. 3.1 illustrates the MOKE setup. The principle of MOKE is that the rotation of the linear polarized light beam during reflection from a

magnetized specimen. The amount of rotation depends on the direction and magnitude of the magnetization relative to the plane of incidence of the light beam. As shown in Fig. 3.1, the linear polarized He-Ne laser light by polarizer is introduced into sample located at the center of the electromagnet. If the sample is magnetized by the field, the induced magnetization of the sample would change the dielectric constant tensor of the sample from diagonal-only form to non-diagonal form. This complex tensor would interact with the linear polarized light, and the reflected light from the sample thus has the elliptical polarization. One can tune the magnetization of the sample by controlling the applied field to change the ellipticity and the tilted angle of the elliptical reflected light from the sample. In our setup, the reflected light is guided into another linear polarizer called analyzer, and then into a photo-diode. Theoretically, the reflected light induced the photo-diode voltage, which is called the Kerr intensity, is proportional to the magnetization of the sample. Therefore, we can measure the hysteresis loop of the sample.

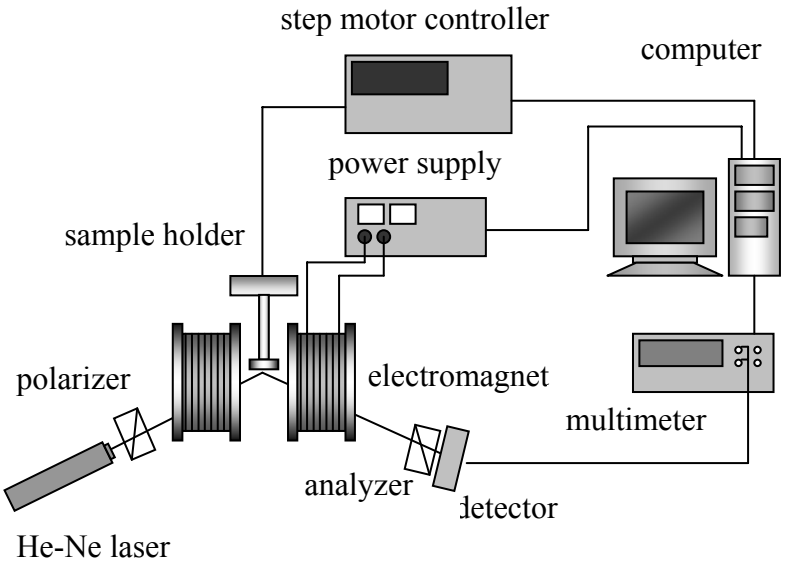

Fig. 3.1. Schematic illustration of the MOKE setup.

Vibrating Sample Magnetometer (VSM)

The principle of VSM is based on the flux change in a coil when the sample is vibrated near it. Fig. 3.2 illustrates the VSM setup. The large electromagnet provides a uniform DC field to the magnetic sample. The emanating magnetization is then measured by vibrating the sample to produce a flux change and therefore to induce a voltage in the pickup coils mounted on both sides of the magnet pole pieces. The coil output voltage is combined with the output from the displacement transducer to produce a magnetization signal. As a result, variations in vibration amplitude and frequency are cancelled out. Then, the electromotive-force signal is detected, by a lock-in amplifier, and transmitted along with the applied field signal to a computer to generate a

hysteresis loop.

The VSM used in the studies, produced by DMS (Digital Measurement Systems, INC), has many special features, such as computer control, automatic data acquisition, and temperature-controlled measurement. The samples can be measured within the temperature range of 100 to 1000 K. A magnetic field up to 16 kOe can be applied to the sample in the measurements. In addition, the VSM system is well suited for measuring major and minor hysteresis loops, initial magnetization curves, and remanent magnetization curves.

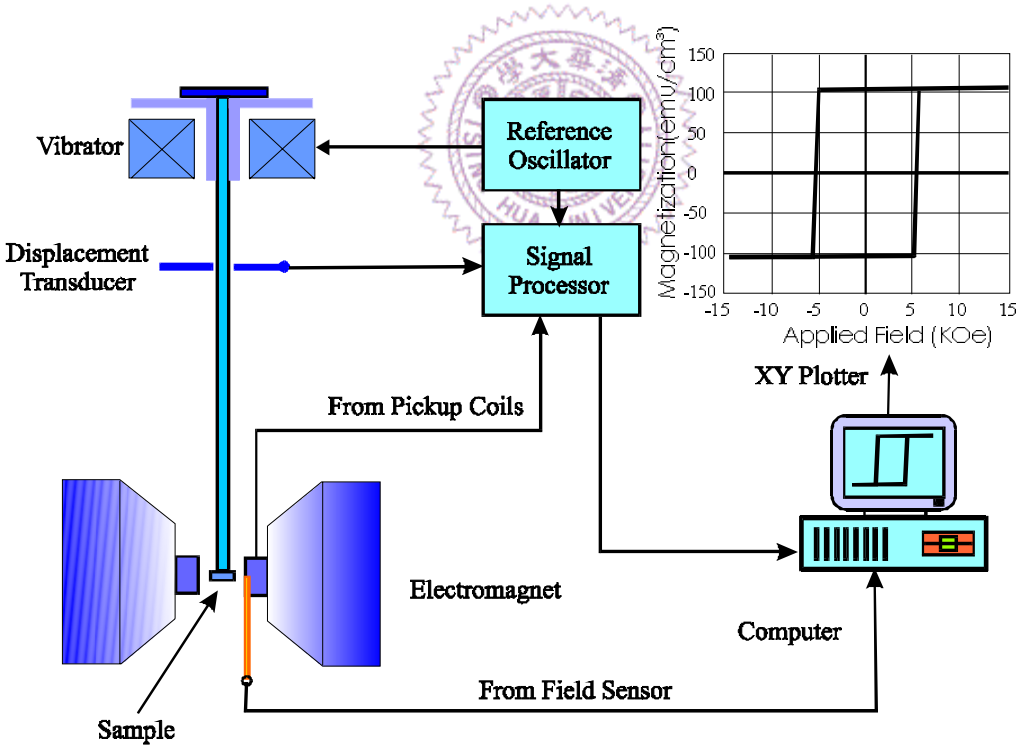

Fig. 3.2. Schematic illustration of the vibrating sample magnetometer (VSM).

X-Ray Magnetic Circular Dichroism (XMCD) Spectroscopy

X-ray Magnetic Circular Dichroism (XMCD) is considered to be one of the most important discoveries in the field of magnetism in the last two decades. It was first suggested by Erskine and Stern in 1975 [1]. The first experiments with circularly polarized x-rays are performed in the high energy range by Schütz *et al*. in 1987 [2]. The XMCD measurement has several capabilities that are not afforded by traditional magnetic analysis techniques. Its foremost strengths are the element-specific, quantitative determination of spin and orbital magnetic moments and their anisotropies [3]. Other strengths are the chemical sensitivity [4], the element-specific imaging capability [5], and its high sensitivity [6,7].

In the XMCD measurement of transition metals, typically, *L-edge* X-ray spectrum was detected, which can best probe the properties of 3d electrons. As shown in Fig. 3.3 [7], the *L*-edge spectrum contains two main absorption peaks of L_3- and L_2-edges which are respectively associated with excitation of $2p_{3/2}$ and $2p_{1/2}$ core electrons to unfilled 3d states. The *L*-edge absorption spectra are characterized by strong absorption resonances, so-called white lines, near the L_3 and L_2 thresholds [7]. The sum of the L_3 and L_2 absorption intensities, denoted I_{L3} and I_{L2}, is proportional to the number of d holes related with the spin moments, as shown in Fig. 3.3. In addition, the spectrum detection affords the capability of element-specific measurement because the *L*-edge position depends strongly on atomic number.

The use of circularly polarized X-rays opens the door for X-ray-based spectroscopy studies of magnetic materials and structure. The basic concept of XMCD spectroscopy is easily understood if we assumed that the d shell has only a spin moment. To measure the difference in the number of d holes with up and down spins, we need to make the X-ray absorption process spin-dependent. Since spin flips are forbidden in electric dipole transitions, spin-up (spin-down) photoelectrons from the p core shell can only be excited into spin-up (spin-down) d hole states. Hence, if one could preferentially generate spin-up photoelectrons in one measurement and the spin-down in another, the difference of the transition intensity in the spectra would simply reflect the difference between up and down holes in the d shell. i.e. the spin moment. This is done by use of right or left circularly polarized photons which transfer their angular momentum to the excited photoelectrons and the difference between the spectra of right- and left-circularly-polarized X-ray is the XMCD spectrum [8,9].

The XMCD effect is quantitatively related to the amounts of magnetic moments and to the anisotropies of the spin density and orbital moments [7,9,10]. The maximum dichroism effect is observed if the photon spin direction and the magnetization directions are parallel or anti-parallel. When the photon spin and the magnetization directions are perpendicular, the resonance intensities at the L_3 and L_2-edges lie between those obtained for parallel and anti-parallel alignments. Thus, the size of the dichroism effect can be considered as a function of cos θ, where θ is the angle between the photon spin and the magnetization direction. The L_3 and L_2

resonance intensities and their differences for parallel and anti-parallel orientation of photon spin and magnetization directions are quantitatively related by sum rules [7,8] to the number of d holes and the size of the spin and orbital magnetic moments. Angular-dependence measurements in external magnetic fields give the anisotropies of the spin density and orbital moment.

In this study, XMCD measurements were made at the Dragon beamline at the Synchrotron Radiation Research Center in Taiwan. The energy resolution of incident light was set to be 0.5 eV and the XMCD spectra were obtained in a total electron yield mode with an 80 Å probing depth. The samples were introduced in an UHV experimental chamber. The pressure during the measurements was below 1×10^{-9} Torr, and the sample temperature was varied from 300 K to 10 K.

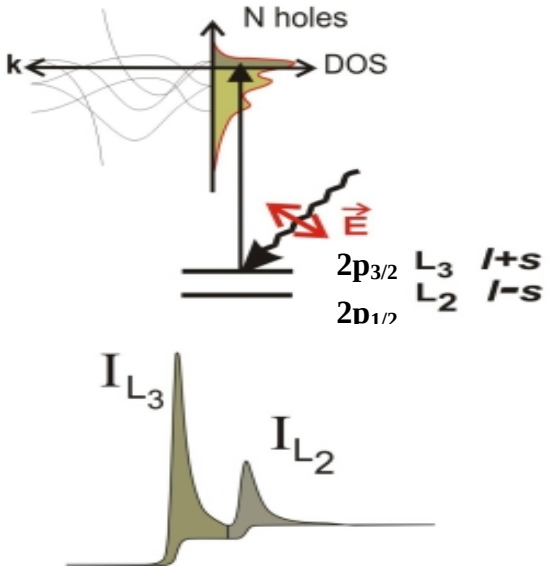

Fig. 3.3. Electronic transitions in conventional L-edge x-ray absorption [7].

3.1.b Transport Measurements

The transport properties of GMR or TMR multilayers are measured by 4-point method in this dissertation. In the 4-point measurement, one can obtain the correct sample resistance by eliminating the contact resistance and spreading resistance. The magnetoresistance measurement system, including GMR and TMR, is shown as Fig. 3.4. The magnetic field in this system is controlled precisely by the bi-polar current source. This setup of electromagnet can obtain a magnetic filed solution of 0.1 Oe and a maximum field of 600 Oe.

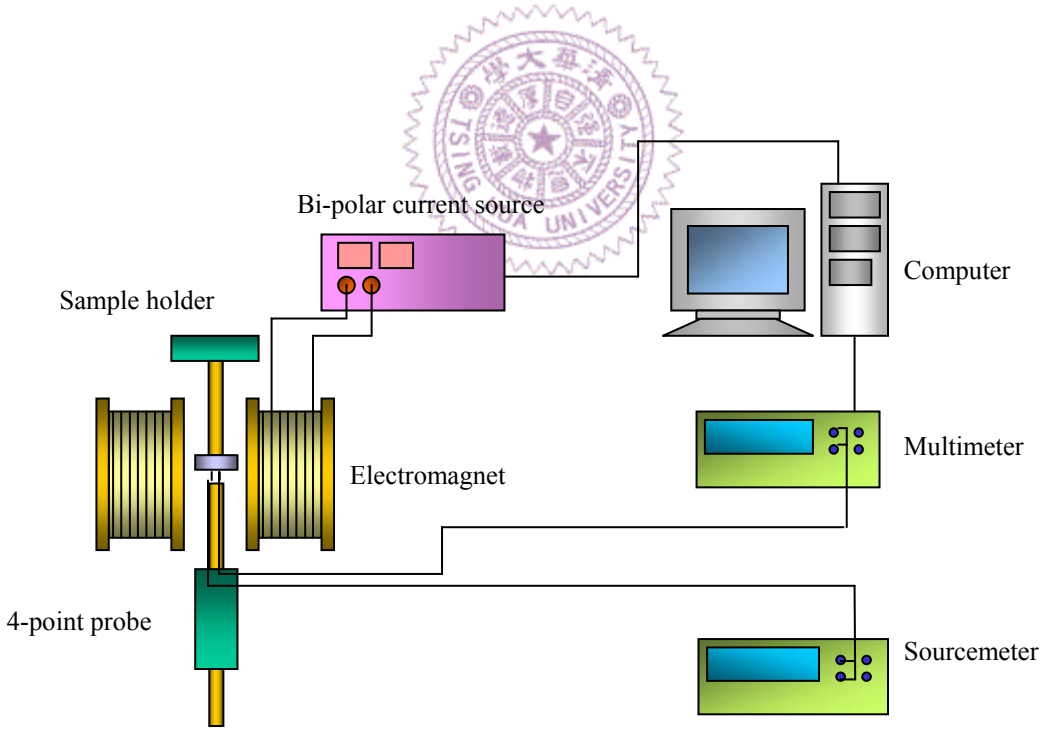

Fig. 3.4. Schematic illustration of the magnetoresistance measurement system.

We used two different kinds of measurement geometry in this dissertation. For GMR multilayers, the resistance measurements are carried out in a conventional geometry that the electric current direction is in the film plane, which is called CIP geometry (current in plane). On the other hand, the resistance measurements of TMR multilayers are measured along the normal direction to the plane, which is called CPP geometry (current perpendicular to plane). The details of CIP and CPP measurements are described as following:

CIP (Current In Plane) for GMR

The CIP geometry is shown as Fig. 3.5. The CIP geometry is usually carried out for thin film specimens with metallic conductivity. Although, the giant magnetoresistance would seem to be present only where current is passed perpendicular to the film planes (CPP). It is indeed true that the GMR effect is largest for CPP geometry, but it is also sizeable for current CIP geometry due to diffusive current between the layers. On the other hand, the CPP geometry is very inconvenient in GMR measurement because the resistance of metallic films in CPP geometry is extremely small. Therefore, we use the CIP geometry for GMR effect measurement in the dissertation.

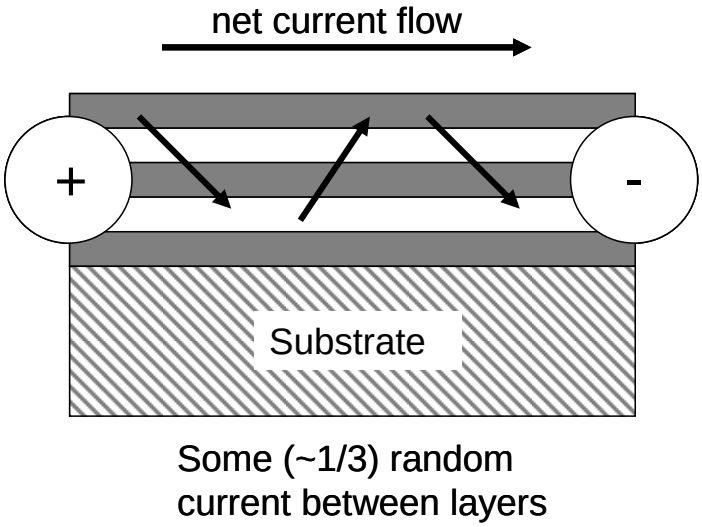

Fig. 3.5. CIP geometry for GMR measurement. In CIP geometry, diffusive currents are present which cross the interfaces, despite the fact that the net current direction is in the planes.

CPP (Current Perpendicular to Plane) for TMR

Since the current must be flowed through the high-resistance tunnel barrier in TMR junctions, the current direction must be designed to be perpendicular to the TMR film plane, as shown in Fig. 3.6. This geometry is called the current perpendicular to the plane (CPP). If one considers that the potential distribution of the two electrodes is uniform, this means that the electrodes resistance could be neglected, the current would tunnel from one electrode to another one uniformly. Combining an external applied field, therefore, we can obtain the magnetoresistance of TMR junctions.

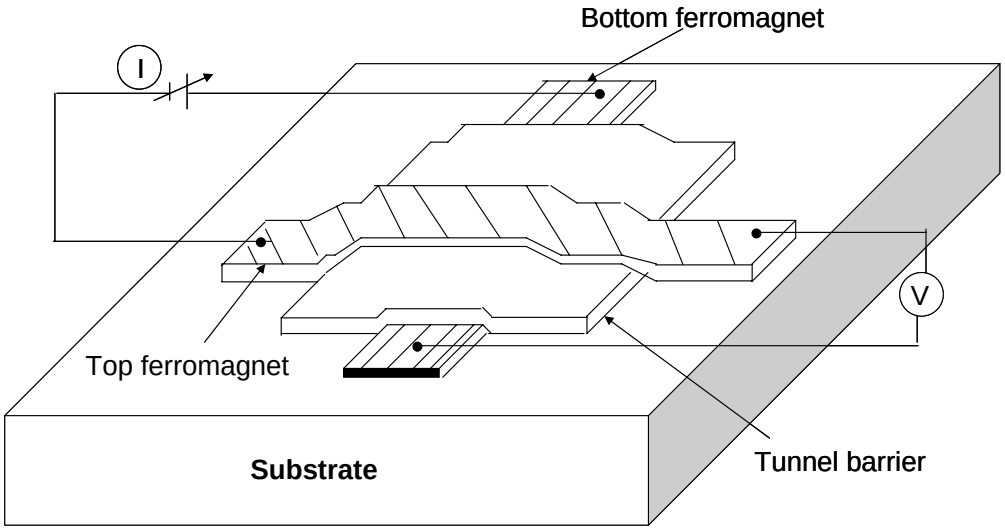

Fig. 3.6. CPP geometry for TMR measurement.

3.1.c Material and Structural Characterizations

In our studies, the structure of multilayers was characterized by X- ray diffraction (XRD) with the wavelength of Cu Kα. Since the NOLs in GMR spin valves and tunnel barrier in TMR junctions are just 10~20 Å, the high resolution transmission electron microscopy (HRTEM) is used to investigate the interface condition in GMR or TME multilayers. In addition, the nano-beam energy dispersive X-ray spectrometer (EDS) and electron energy loss spectra (EELS) attached to TEM were used for investigating the composition of each layer.

3.2 Film Deposition

3.2.a Ion Beam Deposition System

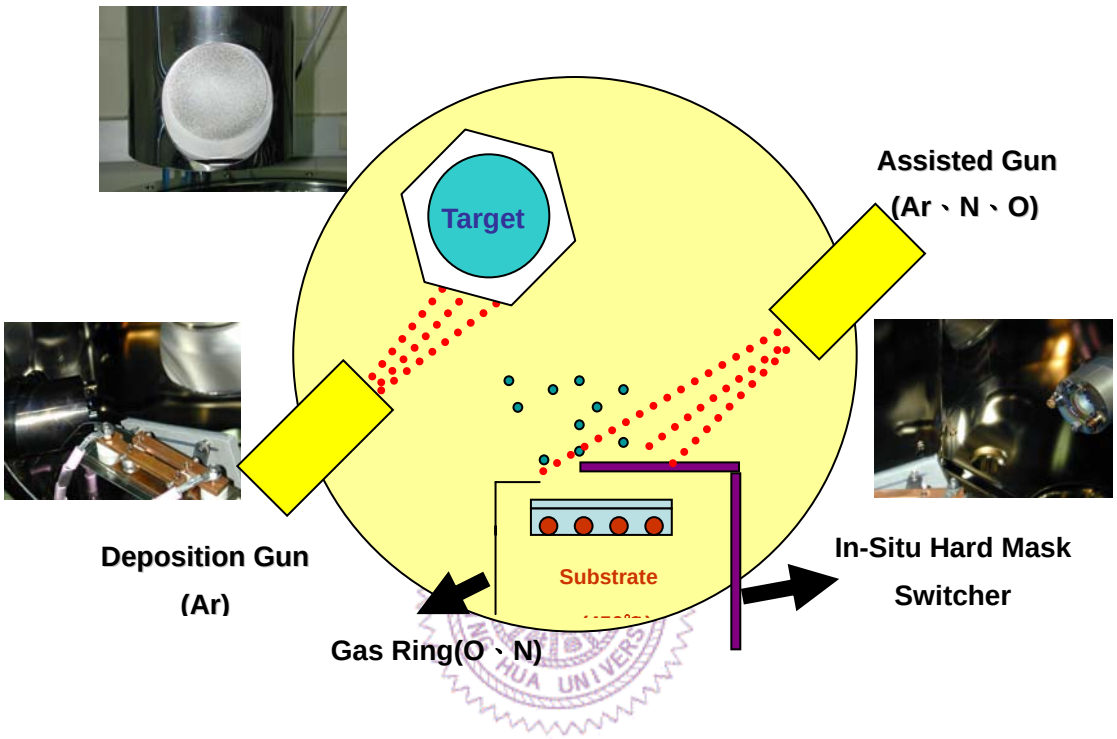

Fig. 3.7. Ion beam deposition system.

In this thesis, all the samples were prepared by the ion beam deposition (IBD) system, as shown in Fig. 3.7. This system contains two parts, the main chamber and loading chamber. Before depositing the sample, we use the transfer arm to put the sample into the main chamber from the loading chamber and then the vacuum system, including a mechanical, a turbo, and a cryo pump, pumps the main chamber down to the base pressure of 2×10^{-7} Torr. Subsequently the 6-embedded-target holder rotates for the deposition of the multilayers.

In the main chamber, it is equipped with the ion gun which can supply the different ion source like Ar, N, and O to tailor the quality of the thin films. It is its advantage that the ion beam deposition can independently operate the excited energy of the incident ion source, higher than other physical vapor deposition like the magnetron sputtering system, at sufficiently low pressure during deposition.

Since the working pressure of IBD is 10^{-4} Torr, this low working pressure reduces the number of collisions between sputtered atoms and gas ions. As shown in the Fig. 3.8, the sputtered atom has higher kinetic energy with the lower working pressure [11]. In addition, the beam voltage of the IBD system can be independently controlled regardless of working pressure and can be raised to 1500 V. Consequently, the IBD system can provide relativity high incident energy of sputtered atoms compared to other deposition method. The energy given by the ion beam system is high enough to reduce the temperature needed for the formation of the Fe_3O_4 and ZnCoO phase.

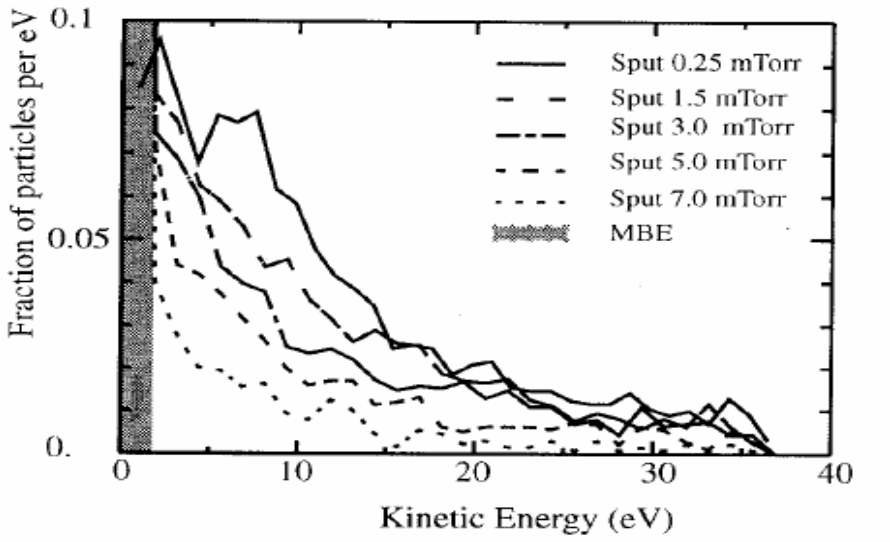

Fig. 3.8. Energy distribution of sputtered atoms at different working pressure [11].